Journal Pre-proof

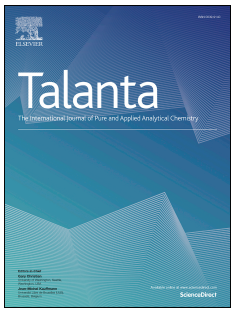

A novel strategy for detection of small molecules based on aptamer/gold nanoparticles/graphitic carbon nitride nanosheets as fluorescent biosensor

Maryam Shirani, Heibatullah Kalantari, Mohammad Javad Khodayar, Maryam Kouchak, Nadereh Rahbar

PII: S0039-9140(20)30526-9

DOI: https://doi.org/10.1016/j.talanta.2020.121235

Reference: TAL 121235

To appear in: *Talanta*

Received Date: 28 April 2020

Revised Date: 31 May 2020

Accepted Date: 31 May 2020

Please cite this article as: M. Shirani, H. Kalantari, M.J. Khodayar, M. Kouchak, N. Rahbar, A novel strategy for detection of small molecules based on aptamer/gold nanoparticles/graphitic carbon nitride nanosheets as fluorescent biosensor, *Talanta*, https://doi.org/10.1016/j.talanta.2020.121235.

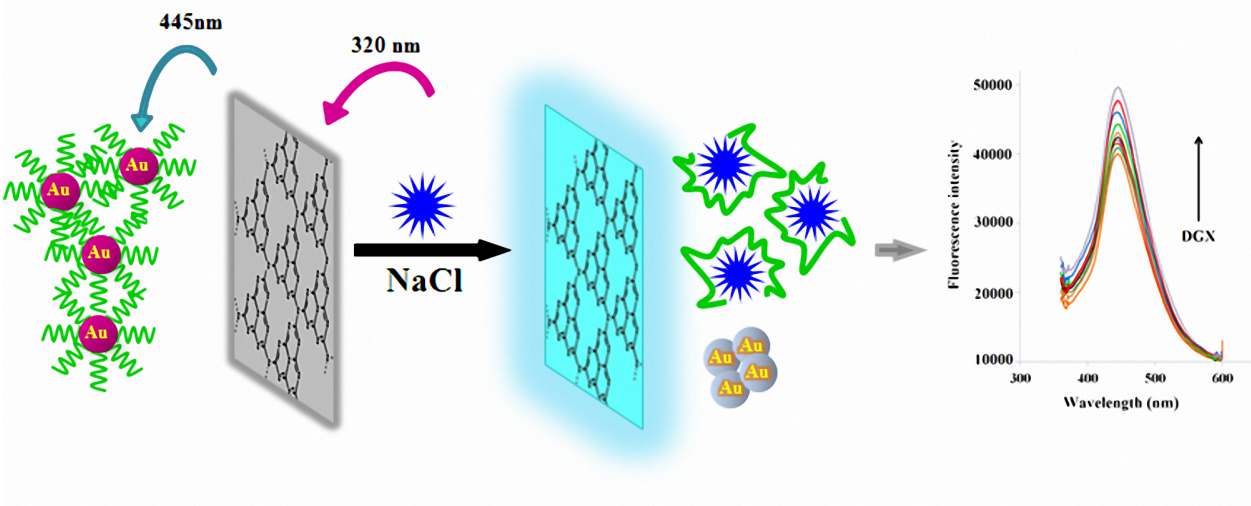

A novel strategy for detection of small molecules based on aptamer/gold nanoparticles/graphitic carbon nitride nanosheets as fluorescent biosensor

Maryam Shirani [a,b], Heibatullah Kalantari [a,b], Mohammad Javad Khodayar [a,b], Maryam Kouchak [c,d], Nadereh Rahbar [c,e,*]

[a]Toxicology Research Center, Ahvaz Jundishapur University of Medical Sciences, Ahvaz, Iran

[b] Department of Toxicology, School of Pharmacy, Ahvaz Jundishapur University of Medical Sciences, Ahvaz, Iran

[c] Nanotechnology Research Center, Ahvaz Jundishapur University of Medical Sciences, Ahvaz, Iran

[d] Department of Pharmaceutics, School of Pharmacy, Ahvaz Jundishapur University of Medical Sciences, Ahvaz, Iran

[e] Department of Medicinal Chemistry, School of Pharmacy, Ahvaz Jundishapur University of Medical Sciences, Ahvaz, Iran

* Corresponding author: Nadereh Rahbar, Department of Medicinal Chemistry, Ahvaz Jundishapur University of Medical Sciences, Ahvaz, Iran.

Tel: +98 61 33738378

Fax: +98 61 33738381

E-mail addresses: n_rahbar2010@ajums.ac.ir

n_rahbar2001@yahoo.com

ABSTRACT

Herein, a novel ultrasensitive strategy has been developed by designing a label free fluorescent nano-aptasensor for monitoring of small moecules in human plasma. In this nano-aptasensor, graphitic carbon nitride nanosheets were used as fluorescent probe. The fluorescence intensity of the probe was decreased by interaction between graphitic carbon nitride nanosheets and label-free aptamer/gold nanoparticles conjugate, via Fluorescence resonance energy transfer mechanism. Upon addition of the analyte, the fluorescence of graphitic carbon nitride nanosheets was restored due to the aptamer/analyte interaction, and the aggregation of gold nanoparticles in the presence of salt. The influence of various factors on sensing method was investigated, and under the approved conditions, the fluorescence signal showed a linear relation with Digoxin concentration in the range of 10-500 ng L^{-1} with limit of detection down to 3.2 ng L^{-1} relative standard deviations for 25, 100 and 500 ng L^{-1} of analyte concentrations were 2.6, 4.0 and 6.5%, respectively. This strategy provided a simple, rapid, cost effective and reproducible experimental model, with successful application for determination of Digoxin in plasma samples without any pretreatment steps.

Keywords: Aptamer; Gold nanoparticles; Graphitic carbon nitride nanosheets; Biosensor; Digoxin.

1. Introduction

Aptamers as artificial single-stranded nucleic acids (ss-DNAs) are the emerging class of ligands which have been known as alternative to antibodies. Aptamers can be easily tagged with the variety of functional groups, dyes and biomolecules, and unlike antibodies, they do not lose their activity. In addition, minimum immunogenicity, low production cost, small size, thermal stability and chemical robustness are the other advantages of aptamers in comparison to antibodies. They can fold into the secondary structures and bind to certain targets such as small molecules, proteins, nucleic acids, and even entire cells with high affinity and specificity via non-covalent binding. Upon binding to its target, conformation of ss-DNA often changes into stem-loop, hairpin, G-quadruplex, pseudoknot or bulge structures [1-3]. These unique features of ss-DNAs make them the ideal candidate for sensing applications and therefore, a number of aptasensors have been developed for detection of various analytes using spectrofluorimetry [4-6], colorimetry [7, 8], and electrochemical methods [9-12]. Recently, Aptamer-based nanosensors are becoming a promising alternative to common sensors for detection of small molecule.

Ultrathin graphitic carbon nitride nanosheets (g-C_3N_4NS) (Fig. S1) are a relatively new class of fluorescent carbon-based nanomaterials, which have recently attracted great attention due to their excellent features including high fluorescence quantum yield and biocompatibility, chemical inertness, low cytotoxicity and cost, and water solubility. These nanosheets are simply synthesized by exfoliating bulk g-C_3N_4 in water without the need for further treatments such as oxidation. Although bulk g-C_3N_4 is fluorescent, 2D g-C_3N_4NS show enhanced photoresponse with respect to

bulk material. Benefiting from these nanomaterials, we proposed the systems for the analysis of some analytes [13, 14]. The intrinsic blue fluorescence emission of g-C_3N_4 under UV light has also been used for developing new detection methods for a number of analytes [15-18]. On the other hand, it is well known that ss-DNAs can easily adsorb on the surface of g-C_3N_4NS and bind via π-π stacking and hydrophobic interactions [19]. Interaction between ss-DNAs and g-C_3N_4NS has shown great potential in various analytical applications [20, 21, 15, 22].

Gold nanoparticles (AuNPs) are widely used as optical sensors due to their surface plasmon resonance property. AuNPs with ruby red color can strongly absorb green light at about 520 nm, related to the frequency at which a plasmon resonance takes place [23]. Intense colors and UV–Vis spectrum of these nanoparticles are dependent on their shape, size, dielectric properties, and interactions between the nanoparticles and their environment [24]. Today, it is well known that the level of particle separation can alter the optical properties of AuNPs. Also, it has been found that bare nanoparticles immediately aggregate after addition of salt (0.1 mol L^{-1} NaCl) in the colloidal suspension and their color is changed to purple. However, in the presence of ss-DNA (without any modification), AuNPs are stabilized against salt-induced aggregation via adsorption of nucleic acid sequences on negatively charged nanoparticles. This phenomenon depends on temperature and DNA sequence length, and no change is observed in the color of DNA-functionalized nanoparticles up to 2.5 mol L^{-1} of NaCl [23, 25, 26, 27]. Recently, ss-DNA functionalized AuNPs have been employed in a number of molecular recognition modes providing new sensors for specific and sensitive detection of proteins, nucleic acids, metal ions, small organic molecules, or even cells [1, 26, 27-30].

Fluorescence resonance energy transfer (FRET) is known as nonradiative energy transfer between a “FRET pair” (emitter and absorber). When emitter-absorber pair is properly oriented and luminescence spectrum of the emitter is overlapped with the absorption spectrum of the absorber, this process can be occurred and therefore, the luminescence of the emitter is quenched. In the last decade, this phenomena has been extensively used as a biosensing tool and a large number of nanomaterial/aptamer based FRET methodologies has been developed owing to their easy operation, less expense and suitability for on-site detection [31]. It is well documented that AuNPs act as the energy acceptor with the high energy transfer rate from energy donors such as dyes and quantum dots, leading to luminescence quenching of these emitters in FRET systems [32-34].

Digoxin (DGX) as a cardiac glycoside-type drug is the most commonly used to treat heart failure and certain cardiac arrhythmias (Fig. S2). This drug is characterized by a narrow therapeutic range (typically 1–2 µg L^{-1} in serum) showing serious side effects in concentrations above 2.8 µg L^{-1}. Thus, selective and sensitive detection of digoxin and control of its concentration level in the serum sample is very important. According to the literature, a few studies have been accomplished in developing aptamer-based sensors for detection of DGX [35-37].

In this work a fast, simple, highly selective, and sensitive strategy for detection of small molecules based on fluorescence quenching of g-C_3N_4NS by DNA-functionalized AuNPs has been introduced for the first time. This nano-sensor is used for direct detection of digoxin as a model molecule, in human plasma samples.

2. Experimental

2.1. Materials

DGX aptamer with the sequence of 5- AGCGAGGGCGGTGTCCAACA GCGGTTTTTTCACGAGGAGGTTGGCGGTGG-3 was supplied by Takapouzist Company (Tehran, Iran). All solutions were prepared using deionized water. Melamine was supplied by Samchun Chemicals Company. DGX was obtained from Sigma–Aldrich and a stock solution of 100 mg L^{-1} was prepared by dissolving 0.01 g of DGX in 8 mL ethanol and diluting to 100 mL in a volumetric flask with deionized water. More diluted solutions were daily prepared using this stock solution. $HAuCl_4$. $3H_2O$ and tri-sodium citrate were purchased from Merck (Darmstadt, Germany).

2.2. Instrumentation

Fluorescence spectra and intensities of the samples were recorded using a Termo SCIENTIFIC-LUMINA (America) fluorescence spectrometer. A Shimadzu model UV-1650PC UV/Visible spectrophotometer (Japan) was employed for the UV-Vis spectrum of g-C_3N_4NS and AuNPs spectra. The Fourier transform infrared (FTIR) spectra were obtained on a Bruker spectrometer (model Tensor 27, Germany) Transmission electron microscopy (TEM) images of the samples were collected using an EM208S (PHILIPS) instrument. The atomic force microscopy (AFM) image of g-C_3N_4NS was obtained using a Nanowizard II instrument (Germany). Dynamic Light Scattering (DLS) analysis was used to determine the particle sizes of AuNPs and aptamer/AuNPs using Qudix, Scatteroscope I system (Korea) instrument. The bulk g-C_3N_4 was liquid exfoliated using an ultrasonic bath (Elma, Germany). The pH values were adjusted with a Metrohm pH-meter model E520 (Switzerland).

2.3. Preparation of g-C_3N_4 NS

The bulk graphitic carbon nitride (g-C_3N_4) was prepared by polymerization of melamine in the semi-closed system as reported in previous work [13] . In brief, melamine was heated at 600 °C for 4 h under air condition with a ramp rate of about 3 °C/min for the heating process in a porcelain crucible. The obtained light yellow product was bulk g-C_3N_4. Nanosheets of g-C_3N_4 were prepared by a liquid exfoliating method. 50 mg of bulk g-C_3N_4 powder was dispersed in 50 mL of deionized water, and the mixture was sonicated for 16 h. After creating a yellow suspension, the produced suspension was centrifuged at 5000 rpm for 10 min to remove the residual un-exfoliated g-C_3N_4 or large-sized nanosheets (Fig. 1A). TEM, IR, and AFM techniques were used to identify the composition and morphology of the synthesized g-C_3N_4NS.

Position of Fig. 1

2.4. Synthesis of AuNPs

For synthesizing the gold nanoparticles with a size of about 20 nm, trisodium citrate was used as the reducing agent for the reduction of $HAuCl_4$. Briefly, 100 mL of $HAuCl_4$ solution (0.25 mmol L^{-1}) was heated to boiling and then, 3 mL of a 1% trisodium citrate solution was added quickly. After 5 minutes, the color changed from pale yellow to gray and finally changed to deep red. Then, the solution was stirred to room temperature for 10 min and stored in refrigerator at 4°C (Fig. 1B). The concentration of the synthesized nanoparticles was 2 nmol L^{-1} [24]. In this method colloidal AuNPs are stabilized by the adsorption of citrate ions on their surface. The citrate capped AuNPs present high stability and optical sensitivity [38].

2.5. Fluorimetric sensing procedure of DGX

Firstly, 200 µL of as prepared AuNPs were mixed with 20 µL DGX aptamer (0.8 µmol L^{-1}) solution and stirred for 5 min. Then the mixture was added into the solution consist of 200 µL of g-C_3N_4NS and 100 µL of NaCl solutions and stirred for another 5 min. Then, the solution was diluted up to 1.5 mL, and the fluorescence intensities of the solution were recorded in the absence and presence of successive concentrations of DGX after 5 min. The fluorescence spectrum of the g-C_3N_4NS was obtained within the wavelength region from 360 to 600 nm. The excitation and maximum emission wavelengths were 320 and 445 nm, respectively [14]. The fluorescence intensity of blank solution containing g-C_3N_4NS, aptamer and AuNPs (F_0) was obtained and the analytical data were gathered based on the difference between the fluorescence intensities of the sample solution containing DGX (F) and blank solution ($F-F_0$). All the obtained data were the averages of three assays. A schematic presentation of the analytical protocol is illustrated in Fig. 1C.

2.6. Real human plasma samples

The plasma samples were supplied by Blood Transfusion organization (Ahvaz, Iran). 30 µL of each human plasma sample spiked with DGX standard solution at the desired concentration and subjected to the optimized method without any preparation or treatment step.

3. Results and discussion

3.1. Principle of detection: on-off-on mechanism in sensing probe

AuNPs and g-C_3N_4NS were used to direct determination of small molecules with the change of the relative fluorescence intensity of the system. After addition of DGX aptamer into the AuNPs suspension, the aptamer adsorbs efficiently on citrate-coated AuNPs. This phenomenon can protect the AuNPs against salt-

induced aggregation [25]. On the other side, it is well known that inherent fluorescence of g-C_3N_4NS via electronic transition between n-nonbonding (HOMO) and p-anti-bonding orbitals (LUMO) is attributed to the sp^2-bonded C-N in conjugated tri-s-triazine rings [39, 40]. As mentioned previously, g-C_3N_4NS exhibit a single peak fluorescence spectrum with the maximum intensity at 450 nm. By adding the aptamer/AuNPs conjugate into g-C_3N_4NS suspension (containing appropriate amount of NaCl), the fluorescence intensity decreases due to the close interaction between g-C_3N_4NS and AuNPs via FRET mechanism [32]. In the other word, a sufficient overlap is occurred between the surface plasmon resonance spectrum of AuNPs and the emission spectrum of g-C_3N_4NS and hence, quenching interaction is observed (Fig. 2) [41, 34]. However, upon addition of DGX into the solution, the fluorescence of g-C_3N_4NS is recovered because of the aptamer/DGX binding and AuNPs aggregation in the presence of salt. Besides, reversibility of aptamer/AuNPs and AuNPs/g-C_3N_4NS bindings is revealed in the restoration of fluorescence intensity of g-C_3N_4NS by DGX.

Position of Fig. 2

3.2. Characterization

The data obtained from particle size analyzer (DLS) showed that the most probable diameters of AuNPs and aptamer functionalized AuNPs are about 20 and 90 nm, respectively (Fig. S3). TEM micrographs of AuNPs in the presence of NaCl and aptamer with NaCl are shown in Fig. 3A. As seen, the obtained results, besides confirming the DLS results concerning the particle size of AuNPs, show the phenomenon of salt induced aggregation of AuNPs in the presence of NaCl (Fig. 3A, image a), and their protection against this phenomenon in the presence of aptamer and NaCl (Fig. 3A, image b). Moreover, as shown in Fig. 3B, the TEM

and AFM images of g-C_3N_4NS reveal its planer shape with a thickness of around 2 nm and a size of about 100 nm. The FTIR spectra were obtained for AuNPs, DGX aptamer, aptamer/AuNPs conjogate, and aptamer/AuNPs/g-C_3N_4NS mixture, as shown in Fig. 3C. FTIR spectrum of AuNPs (Fig. 3C, spectrum a) features the characteristic peaks at 618, 841, 1078, 1396, 1587 cm^{-1}. The peaks at 1396 cm^{-1} and 1587 cm^{-1} are attributed to carboxylate symmetric and asymmetric stretching bands of carboxylate group (COO^-) in citrate ions, respectively. Besides, the peaks belonging to C–O stretching and C–H out of plane vibrations bands of citrate ion are appeared at about 1078 cm^{-1} and 841 cm^{-1} [38]. The peaks below 800 cm^{-1} are related to Au vibrational mode. The frequencies of vibrational modes involving motions of heavy atoms are in this region [42]. FTIR spectrum of DGX aptamer (Fig. 3C, spectrum b) includes the peaks between 3000-3600 cm^{-1} which can be related to the stretching vibrations of –OH and $–NH_2$ group. In this spectrum the peaks between 1500-1650 cm^{-1} are attributed to C=O band and heterocyclic moieties of nucleotide units of ss-DNA structure [43]. Furthermore, the peaks below 1000 cm^{-1} are assigned to the vibrations of the phosphate groups of aptamer [42]. FTIR spectrum of g-C_3N_4NS presents a sharp and intense absorption band at 806 cm^{-1} attributed to the vibration of triazine rings. Besides, it shows some peaks in the region from 1235 to 1645 cm^{-1} as well as 3071 to 3284 cm^{-1} originated from typical stretching modes of either trigonal C-N(-C)-C or bridging C-NH-C, and N-H and O-H stretching bands, respectively [38, 44, 45]. FTIR spectra of aptamer/AuNPs and aptamer/AuNPs/g-C_3N_4NS (Fig. 3C, spectra c and d) represent the expected peaks and the overlapping peaks are observed with slight shifts.

Position of Fig. 3

3.3. Optimization of biosensing conditions

To obtain the best working conditions for the nanobiosensor, the influencing parameters such as concentration of NaCl, aptamer/AuNPs molar ratio, pH, amount of g-C_3N_4Ns, and incubation times for aptamer/AuNPs and aptamer/DGX interactions were optimized. All the presented data in this section were the averages of three determinations. It is noteworthy that the effects of the mentioned parameters on the nanoprobe performance, including concentration of NaCl, aptamer/AuNPs molar ratio, and pH were investigated by spectrophotometric determinations of the solution absorbance at λ=525 nm.

The optimization procedure to determine the best NaCl concentration was performed by introducing various volumes of the salt solution in the range of 20-200 µL into the 650 µL solution containing 200 µL of as prepared AuNPs (2 nmol L^{-1}). The best value of NaCl concentration for maximum aggregation effect was obtained by adding 100 µL of NaCl (100 µmol L^{-1}) solution, and at the higher volumes further decrease was not observed in absorbance of AuNPs in 525 nm (Fig. S4) [23].

To check the aptamer/AuNPs molar ratio influence in the nanobiosensor efficiency, 650 µL of the solutions containing different molar ratios (between 20 and 100) were prepared by mixing various volumes of 0.8 µmol L^{-1} aptamer (10-50 µL) and 200 µL AuNPs (2 nmol L^{-1}) in the presence of NaCl (100 µL of 100 µmol L^{-1}). It was seen that the increase in aptamer/AuNPs ratio, enhances the absorbance of the solution according to the surface plasmon resonance property of AuNPs (Fig. S5). The absorbance reaches its maximum value, and then levels off at the ratio equal to 40 (20 µL) revealing the adsorption of aptamer on the surface of AuNPs and the protection of the nanoparticles against salt aggregation [25].

It was found that pH of solution can effectively influence on assembly or disassembly process of aptamer with the target [23]. The effect of pH on aptamer/DGX assembly and therefore, its influence on salt induced aggregation of AuNPs was investigated in the following conditions: AuNPs, 200 µL; aptamer, 20 µL of 0.8 µmol L^{-1}; NaCl, 100 µL of 100 µmol L^{-1}; DGX concentration, 1 µg L^{-1}, and pH range of 3 to 8 with the final volume of 650 µL. In pHs between 3 and 5, the high absorbance reveal that there is the more affinity between aptamer and AuNPs in this region which prevent nanoparticles from salt induced aggregation (Fig. S6). In lower and higher pHs, a considerable reduction in the absorbance of AuNPs is observed, indicating a decrease in the aptamer affinity to AuNPs or an increase in strength of aptamer/DGX binding. The capped AuNPs by negatively charged citrate ions exhibit an electrostatic barrier for adsorbing aptamers with negative charges. Citric acid pK_as are 3.1, 4.8 and 6.4. In moderate acidic pHs (3-5), the citrate ions on the surface of AuNPs are protonated and the charge repulsion among the negatively charged aptamer and AuNPs reduces which facilitates the aptamer adsorption. This nonionic nature of aptamer adsorption on AuNPs and existence of specific interaction between ss-DNA and AuNPs are proved by previous studies [46]. In addition, in another study it was reported that aptamer affinity to the target decreased in pH about 5, but, the aptamer showed a 100-fold increase in affinity at pH around 7 [47]. Moreover, it is possible that in the highly acidic solution (pH<3), the repulsion forces increase due to the proton uptake by the aptamer phosphate (basic moieties) and AuNPs. By taking these observations and evidences together, it can be concluded that the affinity between the aptamer and AuNPs is relatively poor in the pHs lower than 3 and higher than 5 and conversely, the binding between aptamer and target is stronger [23]. In the other words, the binding of aptamer to target is much stronger than AuNPs in pH about 7, thus the equilibrium is shifted to the target-bound state in the presence of DGX

[48]. From these findings, it can be suggested that the binding affinity between DGX and its aptamer is strongly pH-dependent [47].

To achieve the best amount of g-C_3N_4NS and reaction times, fluorescence of the test solutions was detected by spectrofluorimetry in the excitation and emission wavelengths of 320 and 455 nm, respectively. The effect of the amount of g-C_3N_4NS on the apta-biosensor performance was studied by addition of various volumes of the nanosheets (50-300 µL) into the sample solutions. The best condition was considered as the maximum difference between the fluorescence of g-C_3N_4NS in the absence and presence of aptamer/AuNPs and NaCl. The data was obtained from the difference between the fluorescence intensities of the solutions containing g-C_3N_4NS in the absence (F_0) and presence (F) of aptamer/AuNPs and NaCl (F_0-F). The obtained results indicated that with 200 µL of the nanosheets, the highest fluorescence quenching was observed (Fig. S7).

In this work, reaction times, refer to the incubation times for interactions between aptamer and AuNPs, as well as between aptamer and DGX. Generally, it is most desirable to employ the shortest time in an analytical procedure indicating method performance. Therefore, the time-dependent fluorescence changes upon addition of aptamer/AuNPs conjugate (which was prepared at the various incubation times in the range of 1-20 min) into g-C_3N_4NS and NaCl solution were detected (Fig. S8). In this experimental set, the reaction reached to the equilibrium in 3 min, and higher incubation times did not show considerable improvement on the fluorescence of the solution. Also, the fluorescence changes of the solution containing aptamer/AuNPs/g-C_3N_4NS and NaCl after addition of DGX were determined in the range of 1 to 20 min under optimum conditions (Fig. S9). In this experiments, the reaction reached to the equilibrium in 5 min. According to the

results, one can conclude that the kinetics of the reactions is fast and the equilibrium condition for the aptamer folding processes is obtained in a short time.

3.4. Analytical performance of the biosensor

To evaluate the analytical performance of the proposed biosensor, some figures of merit including linear dynamic range (LDR) of calibration curves (external and in plasma as real sample), LOD (limit of detection), LOQ (limit of quantitation), precision, and accuracy were investigated under optimized conditions. As illustrated in Fig. 4, with the increase of DGX concentrations at ten selected levels (10-500 ng L^{-1}), the fluorescence intensity of the sample solution under optimized conditions as well as the term $F\text{-}F_0$ was linearly increased (Fig. 4, inset b). Inset a in Fig. 4 illustraes the photographs of g-C_3N_4NS under day-light and UV light.

In this work, 3 and 10 times the standard deviation for the blank, divided by slope of external calibration graph (3 and 10 Sb/m) were used to calculate LOD and LOQ, respectively. The analytical features of the method including equations for the external and in real sample standard curves, R^2, LOD, and LOQ are presented in Table 1. The RSD % for 25, 100, and 500 ng L^{-1}, were 2.6, 4.0, and 6.5%, respectively. Compared to the other existing DGX aptasensors, this aptamer/AuNPs/g-C_3N_4NS based nano-bioprobe requires no multistep and complicated procedure and, is quite rapid and cost effective process. Moreover, as seen in Table 2, the analytical parameters of the present sensor are comparable or better than the other previously reported DGX aptasensors.

Position of Fig. 4

Position of Table 1

Position of Table 2

3.5. Selectivity study

Selectivity study is one of the most important steps in evaluating the practical application of the sensor. For this purpose, the selectivity of the designed aptasensor in the presence of some substances such as various heavy metals and common coexisting drugs was examined due to their possible existence in human plasma. The tolerance limit for interference effect in analytical response was considered as the concentration of the substance which causes ± 5 relative error. As seen in Fig. 5, no interfering effects were observed in 700 μg L^{-1} concentration levels of the added substances.

Position of Fig. 5

3.6. Application of the method to the real samples

To check the applicability of the developed fluorescence biosensor for DGX analysis in real matrices, the plasma samples were subjected to the proposed method. At first, the matrix matched standard curve using solutions containing plasma sample fortified for all levels of the external calibration graph was constructed in order to achieve the more accurate results and eliminate the possible matrix effects. Then, its figures of merit were compared with that of the external standard curve which was obtained with standard solutions. These data are presented in Table 1. As seen, their slopes are nearly consistent, and indicate that the sample matrix had no serious influence on the biosensor response. Furthermore, the uniformity of their LDRs, LODs, and LOQs also indicates that the matrix has no significant effect on biosensor performance. Therefore, the external calibration curve was used to examine the accuracy and reliability of the method via recovery data. Hence, DGX at three concentration levels namely 25, 100, and 500 ng L^{-1} was added into the plasma real samples, and analyzed

according to the optimized analytical procedure. Finally, the concentrations of the spiked analyte were interpolated from the external calibration curve. As can be seen from Table 3, the obtained recoveries from the spiked plasma samples are in the acceptable range of 89.2-108.8 % indicating good accuracy of the method and successful applicability of the biosensor for plasma samples without any pretreatment procedure.

Position of Table 3

4. Conclusion

In this work, a novel aptabiosensor on the basis of FRET phenomenon among g-C_3N_4NS and AuNPs has been fabricated for ultra-sensitive determination of small moecules such as DGX (as model molecule) in human plasma samples without any pretreatment step. The fabricated nanobiosensor showed some appealing features such as high selectivity, simplicity, low cost, short assay time, wide dynamic linear range and compatibility with the green chemistry. The linear range of the calibration curve fulfills the requirement for measurement of DGX in narrow therapeutic range. Moreover, the significant benefit of aptamer/AuNPs/g-C_3N_4CN nanoprobe is that with the aid of this probe one can determine very low levels of DGX in plasma without any time consuming extraction or preconcentration procedures. In view of the aforementioned benefits, the developed aptasensor may provide a promising florescence strategy for the determination of DGX in biological environments for diagnostic purposes in medical treatment as well as bioavailability and pharmacokinetic studies.

Acknowledgements

The financial support of this project provided by the Research Council of Ahvaz Jundishapur University of Medical Sciences under grant No. TRC-9720. This paper is extracted from Mrs Maryam Shirani's thesis.

References:

1. Y. Bai, F. Feng, L. Zhao, C. Wang, H. Wang, M. Tian, J. Qin, Y. Duan, X. He, Aptamer/trombin/aptamer-AuNPs sandwich enhanced surface plasmon resonance sensor for the detection of subnanomolar thrombin, Biosens. Bioelectron. 47 (2013) 265-270.

2. J. Ashley, S.F. Li, An aptamer based surface plasmon resonance biosensor for the detection of bovine catalase in milk, Biosens. Bioelectron. 48 (2013) 126-131.

3. J. Xu, Y. Li, L. Wang, Y. Huang, D. Liu, R. Sun, J. Luo, C. Sun, A facile aptamer-based sensing strategy for dopamine through the fluorescence resonance energy transfer between rhodamine B and gold nanoparticles, Dyes Pigments 123 (2015) 55-63.

4. Y. Lan, G. Qin, Y. Wei, C. Dong, L. Wang, Highly sensitive analysis of tetrodotoxin based on free-label fluorescence aptamer sensing system. Spectrochim. Acta Part A 219 (2019) 411-418.

5. H. Li, W. Ahmad, Y .Rong, Q. Chen, M. Zuo, Q. Ouyang, Z. Guo, Designing an aptamer based magnetic and upconversion nanoparticles conjugated fluorescence sensor for screening Escherichia coli in food, Food Control 107 (2020) 106761.

6. Y. Li, J. Wang, B. Zhang, Y. He, J. Wang, S. Wang, A rapid fluorometric method for determination of aflatoxin B1 in plant-derived food by using a thioflavin T-based aptasensor, Microchim. Acta 186 (2019) 214.

7. L. Zhu, S. Li, X. Shao, Y. Feng, P. Xie, Y. Luo, K. Huang, W. Xu, Colorimetric detection and typing of E. coli lipopolysaccharides based on a dual aptamer-functionalized gold nanoparticle probe, Microchim. Acta 186 (2019) 111.

8. B. Lin, Y. Yu, Y. Cao, M. Guo, D. Zhu, J. Dai, M. Zheng, Point-of-care testing for streptomycin based on aptamer recognizing and digital image colorimetry by smartphone, Biosens. Bioelectron. 100 (2018) 482-489.

9. Y.H. Wang, H. Xia, K.J. Huang, X. Wu, Y.Y. Ma, R. Deng, Y.F. Lu, Z.W. Han, Ultrasensitive determination of thrombin by using an electrode modified with WSe_2 and gold nanoparticles, aptamer-thrombin-aptamer sandwiching, redox cycling, and signal enhancement by alkaline phosphatase, Microchim. Acta 185 (2018) 502.

10. Z. Bai, Y. Chen, F. Li, Y. Zhou, H. Yin, S. Ai, Electrochemical aptasensor for sulfadimethoxine detection based on the triggered cleavage activity of nuclease P1 by aptamer-target complex, Talanta 204 (2019) 409-414.

11. L. Zhao, Y. Huang, X. Qi, X. Yan, S. Wang, X. Liang, Nanotetrahedron-assisted electrochemical aptasensor with cooperatively-folding aptamer chimera for sensitive and selective detection of lysozyme in red wines, Anal. Chim. Acta 1095 (2019) 172-178.

12. B. He, X. Dong, Aptamer based voltammetric patulin assay based on the use of ZnO nanorods, Microchim. Acta 185 (2018) 462.

13. N. Rahbar, P. Abbaszadegan, A. Savarizadeh, A sensitive fluorescent sensing strategy for nanomolar levels of metformin using graphitic carbon nitride nanosheets as nanofluoroprobe, Anal. Chim. Acta 1026 (2018) 117-124.

14. N. Rahbar, Z. Salehnezhad, A. Hatamie, A. Babapour, Graphitic carbon nitride nanosheets as a fluorescent probe for chromium speciation, Microchim. Acta 185 (2018) 101.

15. J. Li, H. Wang, Z. Guo, Y. Wang, H. Ma, X. Ren, B. Du, Q. Wei, A "turn-off" fluorescent biosensor for the detection of mercury (II) based on graphite carbon nitride, Talanta 162 (2017) 46-51.

16. M.H. Xiang, J.W. Liu, N. Li, H. Tang, R.Q. Yu, J.H. Jiang, Fluorescent graphitic carbon nitride nanosheet biosensor for highly sensitive, label-free detection of alkaline phosphatase, Nanoscale 8 (2016) 4727-4732.

17. J.W. Liu, Y. Luo, Y.M. Wang, L.Y. Duan, J.H. Jiang, R.Q. Yu, Graphitic carbon nitride nanosheets-based ratiometric fluorescent probe for highly sensitive

detection of H_2O_2 and glucose, ACS Appl. Mater. Interfaces 8 (2016) 33439-33445.

18. J. Han, H.Y. Zou, M.X. Gao, C.Z. Huang, A graphitic carbon nitride based fluorescence resonance energy transfer detection of riboflavin, Talanta 148 (2016) 279-284.

19. Y.M. Wang, J.W. Liu, G.B. Adkins, W. Shen, M.P. Trinh, L.Y. Duan, J.H. Jiang, W. Zhong, Enhancement of the intrinsic peroxidase-like activity of graphitic carbon nitride nanosheets by ssDNAs and its application for detection of exosomes, Anal. chem. 89 (2017) 12327-12333.

20. X. Liu, H. Zhang, Z. Song, L. Guo, F. Fu, Y. Wu, A ratiometric nanoprobe for biosensing based on green fluorescent graphitic carbon nitride nanosheets as an internal reference and quenching platform, Biosens. Bioelectron.129 (2019) 118-123.

21. Q. Wang, W. Wang, J. Lei, N. Xu, F. Gao, H. Ju, Fluorescence quenching of carbon nitride nanosheet through its interaction with DNA for versatile fluorescence sensing, Anal. chem. 85 (2013) 12182-12188.

22. K. Hu, T. Zhong, Y. Huang, Z. Chen, S. Zhao, Graphitic carbon nitride nanosheet-based multicolour fluorescent nanoprobe for multiplexed analysis of DNA, Microchim. Acta 182 (2014) 949-955.

23. S.K. Ghosh, T. Pal, Interparticle coupling effect on the surface plasmon resonance of gold nanoparticles: from theory to applications, Chem. Rev. 107 (2007) 4797-4862.

24. Z. Masoudyfar, S. Elhami, Surface plasmon resonance of gold nanoparticles as a colorimetric sensor for indirect detection of Cefixime. Spectrochim. Acta Part A 211 (2019) 234-238.

25. H. Li, L.J. Rothberg, Label-free colorimetric detection of specific sequences in genomic DNA amplified by the polymerase chain reaction, J. Am. Chem. Soc. 126 (2004) 10958-10961.

26. Z. Luo, J. Zhang, Y. Wang, J. Chen, Y. Li, Y. Duan, An aptamer based method for small molecules detection through monitoring salt-induced AuNPs aggregation and surface plasmon resonance (SPR) detection, Sens. Actuators B 236 (2016) 474-479.

27. D. Tan, Y. He, X. Xing, Y. Zhao, H. Tang, D. Pang, Aptamer functionalized gold nanoparticles based fluorescent probe for the detection of mercury (II) ion in aqueous solution, Talanta 113 (2013) 26-30.

28. Q. Li, Q. Wang, X. Yang, K. Wang, H. Zhang, W. Nie, High sensitivity surface plasmon resonance biosensor for detection of microRNA and small molecule based on graphene oxide-gold nanoparticles composites, Talanta 174 (2017) 521-526.

29. S. Kim, S. Lee, H.J. Lee, An aptamer-aptamer sandwich assay with nanorod-enhanced surface plasmon resonance for attomolar concentration of norovirus capsid protein, Sens. Actuators B 273 (2018) 1029-1036.

30. S. Koyun, S. Akgonullu, H. Yavuz, A. Erdem, A. Denizli, Surface plasmon resonance aptasensor for detection of human activated protein C, Talanta 194 (2019) 528-533.

31. Z.S. Pehlivan, M. Torabfam, H. Kurt, C. Ow-Yang, N. Hildebrandt, M. Yuce, Aptamer and nanomaterial based FRET biosensors: a review on recent advances (2014-2019), Microchim Acta 186 (2019) 563.

32. A. Samanta , Y. Zhou , S. Zou , H. Yan , Y. Liu , Fluorescence quenching of quantum dots by gold nanoparticles: a potential long range spectroscopic ruler, Nano Lett. 14 (2014) 5052-5057.

33. Y. Li, N. Chopra, Gold nanoparticle integrated with nanostructured carbon and quantum dots: synthesis and optical properties, Gold Bull. 48 (2015) 73-83.

34. H. Shan, W. Lumin, H. Chusheng, H. Baoqing, S. Wei, X. Qi, Graphene quantum dot coupled with gold nanoparticle based "off-on" fluorescent probe for sensitive and selective detection of L-cysteine, Microchim. Acta 183 (2016) 1855-1864.

35. A. Sarreshtehdar Emrani, N.M. Danesh, P. Lavaee, S.H. Jalalian, M. Ramezani, K. Abnous, S.M. Taghdisi, Sensitive and selective detection of digoxin based on fluorescence quenching and colorimetric aptasensors, Anal. Methods 7 (2015) 3419-3424.

36. A. Sarreshtehdar Emrani, S.M. Taghdisi, N.M. Danesh, S.H. Jalalian, M. Ramezani, K. Abnous, A novel fluorescent aptasensor for selective and sensitive

detection of digoxin based on silica nanoparticles, Anal. Methods 7 (2015) 3814-3818.

37. H. Elmizadeh, F. Faridbod, M. Soleimani, M.R. Ganjali, G. Rezanejade Bardajee, Fluorescent apta-nanobiosensors for fast and sensitive detection of digoxin in biological fluids using rGQDs: Comparison of two approaches for immobilization of aptamer, Sens. Actuators B 302 (2020) 127133.

38. P. Wulandari, X. Li, K. Tamada, M. Hara, Conformational study of citrates adsorbed on gold nanoparticles using fourier transform infrared spectroscopy, J. Nonlinear Opt. Phys. Mater.17 (2012) 185-192.

39. Z. Zhou , Y. Shen , Y. Li , A. Liu , S. Liu , Y. Zhang , Chemical cleavage of layered carbon nitride with enhanced photoluminescent performances and photoconduction, ACS Nano 9 (2015) 12480-12487.

40. Y. Zhang, Q. Pan, G. Chai, M. Liang, G. Dong, Q. Zhang, J. Qiu, Synthesis and luminescence mechanism of multicolor-emitting g-C_3N_4 nanopowders by low temperature thermal condensation of melamine, Sci. Rep. 3 (2013) 1943.

41. F. Nasrin, A.D. Chowdhury, K. Takemura, J. Lee, O. Adegoke, V.K. Deo, F. Abe, T. Suzuki, E.Y. Park, Single-step detection of norovirus tuning localized surface plasmon resonance-induced optical signal between gold nanoparticles and quantum dots, Biosens. Bioelectron. 122 (2018) 16-24.

42. M. Klähn, G. Mathias, C. Kötting, M. Nonella, J. Schlitter, K. Gerwert, P. Tavan, IR spectra of phosphate ions in aqueous solution: predictions of a DFT/MM approach compared with observations, J. Phys. Chem. A 108 (2004) 6186-6194.

43. C, Acquah, Y.W. Chan, S. Pan, L.S. Yon, C.M. Ongkudon, H. Guo, M.K. Danquah, Characterisation of aptamer-anchored poly(EDMA-co-GMA) monolith for high throughput affinity binding, Sci. rep. 9 (2019) 14501.

44. Q. Han, B. Wang, J. Gao, Z. Cheng, Y. Zhao, Z. Zhang, L. Qu, Atomically thin mesoporous nanomesh of graphitic C_3N_4 for high-efficiency photocatalytic hydrogen evolution, ACS Nano 10 (2016) 2745-2751.

45. Y. Liu, K. Yan, J. Zhang, Graphitic carbon nitride sensitized with CdS quantum dots for visible-light-driven photoelectrochemical aptasensing of tetracycline, ACS Appl. Mater. Interfaces 8 (2016) 28255-28264.

46. X. Zhang, M.R. Servos, J. Liu, Surface science of DNA adsorption onto citrate-capped gold nanoparticles, Langmuir 28 (2012) 3896-3902.

47. C.K.L. Gordon, M. Eisenstein, H.T. Soh, A direct selection strategy for isolating aptamers with pH-sensitive binding activity, ACS Sens. 3 (2018) 2574-2580.

48. P.A. Mirau, J.E. Smith, J.L. Chavez, J.A. Hagen, N. Kelley-Loughnane, R.R. Naik, Structured DNA aptamer interactions with gold nanoparticles. Langmuir 34 (2018) 2139-2146.

49. M.H. Mashhadizadeh, N. Naseri, M.A. Mehrgardi, Digoxin electrochemical aptasensor using ag nanoparticles decorated graphene oxide, Anal. Methods 8 (2016) 7247-7253.

50. M.H. Mashhadizadeh, A. Azhdeh, N. Naseri, 3-Mercapto propionic acid self-assembled on gold nano-particles applied for modification of screen-printed electrode as a new digoxin electrochemical aptasensor using graphene oxide-based signal-on strategy. J. Electroanal.l Chem. 787 (2017) 132-138.

Caption to the figures:

Fig. 1: Graphical illustration for A) synthesis of g-C_3N_4NS, B) fabrication of AuNPs, and C) analytical protocol for aptamer/AuNPs/g-C_3N_4NS sensor in determination of DGX.

Fig. 2: (A) The overlap between fluorescence spectrum of g-C_3N_4NS (a) and absorbance spectrum of AuNPs (b), and (B) the fluorescence spectra of g-C_3N_4NS (100 µL) in the solution consist of aptamer/AuNPs conjugate, in the absence (a) and presence (b) of DGX (500 ng L^{-1}).

Fig. 3: (A): TEM images of a) AuNPs in NaCl 100 µ µmol L^{-1}, b) aptamer/AuNPs in NaCl 100 µmol L^{-1}, (B): a) TEM image of g-C_3N_4NS and, b) AFM image of g-C_3N_4NS (inset image shows the height of the nanosheets). (C): FTIR spectra of a) AuNPs, b) DGX aptamer, c) aptamer/AuNPs, and d) aptamer/AuNPs/g-C_3N_4NS.

Fig. 4: The recovered fluorescence spectra of g-C_3N_4NS in the presence of DGX (10-500 ng L^{-1}). Inset (a): the photographs of g-C_3N_4NS under day-light (left) and UV light (right), and inset (b): the plot of F-F_0 for the standard solutions versus various DGX concentrations (10-500 ng L^{-1}). Condition: AuNPs: 200 µL, aptamer: 20 µL of 0.8 µmol L^{-1}, NaCl: 100 µL of 100 µmol L^{-1}, pH: 7, g-C_3N_4NS volume: 200 µL, incubation time in each step: 5 min.

Fig. 5: selectivity study under the optimal conditions towards some possible interfering species (cation and drug concentrations: 700 µg L^{-1}).

Table 1

Analytical features for determination of DGX by the current aptasensor.

Standard curve	LOD (ng L^{-1})	LOQ (ng L^{-1})	LDR (ng L^{-1})	R^2	Regression equation
External	3.2	10	10 – 500	0.9993	y = 8.94 x + 292.09
In plasma	4.3	10	10 – 500	0.9991	y = 9.20 x + 447.81

Table 2

Performance comparison of aptamer/AuNPs/g-C3N4NS based nano-bioprobe with other reported aptasensors in DGX detection.

Method	Matrices	LDR	LOD	References
Colorimetric aptasensor based on AuNPs	Rat serum	0-30 (nM)	571 (pM)	[35]
Fluorescence quenching based on fluorescent labeled-aptamer	Rat serum	0-30 (nM)	392 (pM)	[35]
Fluorescent labeled-aptasensor based on silica nanoparticles coated with streptavidin	Rat serum	0-60 (nM)	566 (pM)	[36]
Fluorescent aptasensors based on reduced graphen quantum dots (rGODs)	Human plasma and urine	99.5-540 (pM)	29.87(pM)	[37]
Fluorescent labeled-aptasensors based on rGODs and carbon nano tubes	Human plasma and urine	26.5-680 (pM)	7.95 (pM)	[37]
Electrochemical aptasensor	Human plasma	1-100 (pM)	0.3 (pM)	[49]
Electrochemical aptasensor	Human plasma	1-100 (pM)	0.05 (pM)	[50]
Fluorescent label-free aptasensors based on AuNPs and g-C3N4NS	Human plasma	12.8-640.7 (pM) [a]	4.1 (pM) [b]	Present work

[a] 10-500 (ng L^{-1})

[b] 3.2 (ng L^{-1})

Table 3

DGX detection in human plasma by aptamer/AuNPs/g-C_3N_4NS nanofluoroprobe [a].

Sample	Added (ng L^{-1}) [b]	Found (ng L^{-1}) [c]	Recovery (%)
Plasma 1	25	27.2±1.7 [d]	108.8
	100	105.0±5.3	105.0
	500	505.4±8.5	101.1
Plasma 2	25	26.5±1.2	106.0
	100	94.8±4.9	94.8
	500	487.1±10.9	97.4
Plasma 3	25	22.3±1.9	89.2
	100	99.1±5.0	99.1
	500	513.5±11.0	102.7
Plasma 4	25	23.7±1.7	94.8
	100	102.5±4.5	102.5
	500	480.0±9.8	96.0
Plasma 5	25	26.2±1.5	104.8
	100	96.8±4.1	96.8
	500	510.6±9.3	102.1

[a] 30 µL of human plasma was used in the optimized analytical method.

[b] Spiked concentrations of DGX (ng L^{-1}).

[c] Recovered concentrations of DGX (ng L^{-1}).

[d] $\bar{x} \pm s$ (n=3).

In this research:

- A simple and cost effective method is used for the preparation of a nanoprobe and its exploiting for analyte determination without need to the sophisticated instruments.
- The important feature of this bioprobe is its high selectivity toward analyte duo to use of the aptamer.
- The significant benefit of aptamer/AuNPs/g-C_3N_4CN nanoprobe is that with the aid of this probe determination of very low levels of the analyte in plasma is performed without any time consuming extraction or preconcentration procedures.
- The developed nanobiosensor is thoroughly compatible with the green chemistry.
- The linear range of the calibration curve fulfills the requirement for measurement of DGX in narrow therapeutic range (1-2 ppb).
- Ease of the procedure as well as amazing analytical characteristics such wide dynamic range, low LOD, and short operation time compared with most of the other reported methods are the essential features of the method.
- Satisfactory recoveries from real samples are obtained, indicating the potential of the synthesized nanobioprobe for selective and sensitive detection of the analyte in complicated matrices.
- In view of the aforementioned benefits, the developed aptasensor may provide a promising florescence strategy for the determination of DGX or other analytes (by the use of appropriate aptamer) in biological fluids for diagnostic purposes in medical treatment as well as bioavailability and pharmacokinetic studies.

Declaration of interests

I would like to declare on behalf of the authors that they have no known competing financial interests or personal relationships that could have appeared to influence the work reported in this paper.

N. Rahbar

Associate professor in Analytical Chemistry

Ahvaz Jundishapur University of Medical Sciences

Ahvaz

Iran

Credit author statement

Ms. Ref. No.: TAL-D-20-01742

Manuscript title: *A novel strategy for detection of small molecules based on aptamer/gold nanoparticles/graphitic carbon nitride nanosheets as fluorescent biosensor*

The contribution of individual authors to manuscript preparation is defined in terms of the following criteria:

1- Maryam Shirani: Performing the experiments; acquisition and collation of data; writing the original draft preparation

2- Heibatullah Kalantari: Conceptualization; original idea of the research; review and editing of the manuscript

3- Mohammad Javad Khodayar: Conceptualization; interpretation of data; review and editing of the manuscript

4- Maryam Kouchak: Conceptualization; review and editing of the manuscript

5- Nadereh Rahbar: Conceptualization; Development or design of methodology; analysis and interpretation of data; writing, review and editing of the manuscript, critical revision of the manuscript